El Cezeri
Journal of Science and Engineering
ISSN: 2148-3736

Research Article

Testing and Characterization of FBE+ARO Dual Layer Coatings of Welded Steel Pipes

Erman Ferik[1a], Semih Özbey[1b], Gökhan Çil[2c] Mahmut Gel[2d]
[1] Metallurgical and Materials Engineering Department, Marmara University, Istanbul, Turkiye
[2] Erciyas Steel Pipe, Design Center, Düzce, Turkiye

erman.ferik@marmara.edu.tr

DOI : 10.31202/ecjse.1445962
Received: 01.03.2024 Accepted: 11.07.2024
How to cite this article:
Erman Ferik, Semih Özbey, Gökhan Çil, Mahmut Gel, " Testing and Characterization of FBE+ARO Dual Layer Coatings of Welded Steel Pipes", El-Cezeri Journal of Science and Engineering, Vol: 12, Iss: 2, (2025), pp.(127-133).
ORCID: [a]0000-0002-9694-5732; [b] 0000-0001-5582-9973. [c] 0000-0003-0924-3984; [d] 0000-0002-8384-4932.

Abstract : The demand for extended life and outer surface protective coatings in pipelines is steadily increasing. Several coatings are used to protect pipelines against corrosion, impact, and abrasion. In this study, spiral welded steel pipes were coated with fusion bonded epoxy (FBE) for corrosion protection, followed by an abrasion-resistant coating (ARO) to protect the pipe from impact and abrasion. Various tests and characterization analyses were conducted on the coated pipes under different conditions, and they passed successfully, meeting the relevant standards and specifications.

Keywords : steel pipe, corrosion, abrasion, FBE coating, ARO coating

1 Introduction

Large amounts of crude oil, natural gas, and other resources are delivered efficiently and effectively from production locations to refineries and consumer markets. Pipelines are more cost-effective and safer than roads, rails, and ships for transporting freight across cities, countries, and continents. Every day, thousands of kilometers of steel pipelines are installed around the world for a wide range of civil and industrial purposes, forming a network of pipes similar to a vascular network that transports materials for people's natural resources such as petroleum products, natural gas, water, and air. Natural gas, water, air, and petroleum products are all delivered using steel pipes due to their flexibility and strength. If steel pipes are not covered or coated (galvanizing, plating), they corrode quickly [1]–[4].

Corrosion is simply defined as the deterioration of metal caused by chemical or electrochemical reactions that occur between the metal and its surroundings. A metal's corrosiveness is determined by its kind and surroundings. Corrosion is the second-leading cause of pipeline damage. Corrosion can cause industrial closures, product pollution, soil and groundwater contamination, pipeline breaks that result in significant losses of transported commodities, and even fires. Pipeline coating should always be the primary defense against corrosion, and it needs to be supported by a powerful cathodic protection system [5]–[18].

Nowadays, fusion-bonded epoxy (FBE) is almost usually the preferred alternative for pipeline coatings used around the world. This coating is ideal for pipelines due to its numerous benefits. These include a wide operating temperature range (-40°C to 105°C), strong adhesion to the steel substrate, good flexibility, high chemical resistance, low oxygen permeability, and compatibility with cathodic protection [19], [20].

The primary risk with single-layer FBE coating is shipping and handling damage. The thickness of the coating can be raised to improve impact and abrasion resistance. However, the coating's elasticity decreases with thickness. Steel pipes can also be coated with a secondary coating on top of the anti-corrosion coating to protect against pitting, impact, and abrasion during embedding. The abrasion resistant protective coating (ARO) is a topcoat that protects the steel pipeline's primary corrosion coating against abrasion damage during pipeline construction [2], [21].

2 Experimental Methods

2.1 Materials

This study used a 12m long, Ø762 mm diameter steel pipe made from API X70M PSL2 steel grade material utilizing spiral submerged arc welding (HSAW) with a wall thickness of 12.24 mm, often used in natural gas and oil pipes.

Table 1: Chemical characteristics of X70M PSL2 steel pipe.

Chemical Composition (%)					
C	**Si**	**Mn**	**P**	**S**	**Cr**
0.0635	0.221	1.680	0.0100	0.0075	0.136
Mo	**Ni**	**Cu**	**B**	**Nb + V + Ti**	**CEpcm**
0.0053	0.0239	0.0387	0.00053	0.0778	0.167

Table 2: Mechanical characteristics of X70M PSL2 steel pipe

Ultimate Tensile Strength (N/mm^2)	Yield Strength (N/mm^2)	Elongation (%)
675	601	27

Electrostatic spray guns were used to apply two-layers of fusion bonded epoxy coating with thermosetting epoxy powders, the first layer (FBE) designed for corrosion protection and the top layer (ARO) designed for high abrasion, followed by two-layers of abrasion resistance coating in accordance with the relevant standard requirements (CSA Z245.20 series 18 - system 2B) using for plant-applied external fusion bond epoxy coating for steel pipe. The chemical and mechanical characteristics of the welded steel pipe are presented in Tables 1 and 2. Table 3 shows the characteristics of both FBE and ARO coatings.

2.2 Method

Before applying the FBE and ARO coatings, the outer surface of the welded steel pipe was blasted in an automatic blasting station using a mixture of grit and shot in equal proportions. The outer surface of the pipe was then treated using phosphoric acid diluted with water, followed by rinsing with distilled water and drying with compressed air. The blasted pipe surface was heated to 215°C with an induction coil before the external surface coating process was applied. Electrostatic spray guns were used to apply powder epoxy materials to the surface of the heated pipe in a single layer for FBE and ARO coating, respectively.

Following the coating procedure, the pipe surface was cooled with water to allow for the gel time of the coatings. To assess the coating's performance on the coated sample, cross-sectional and interface porosity, interface contamination level, bending, impact, cathodic peeling, and adhesion tests were carried out. The test requirements were determined according to CSA Z245.20 series 18 - system 2B. The coating's surface was photographed and examined with SEM and EDX methods to ascertain its chemical characterization.

3 Results and Discussion

3.1 Surface Preparation Test and Control Results

Prior to blasting, the ambient conditions, including blasting media, acid, and pure water, were examined and measured. The recorded measurements are shown in Table 4.

Surface preparations before and after coating were carried out in accordance with the CSA-Z245.20 series 18 standard. Surface roughness values ranged from 77μ m to $91\mu m$, meeting the acceptable threshold of $50\mu m - 100\mu m$ [22], [23].

Figure 1 depicts images of the surface roughness test, dust test, acid ratio determination test, and blasting media conductivity test measurements taken following surface preparation.

Table 3: FBE and ARO coating characteristics

Product	FBE	ARO
Colour	Red	Grey
Density (g/L)	1470	1590
Particle size (µm)	% 0.32 > 150 % 0 > 250	% 0.60 > 150 % 0 > 250
Thermal Characteristics (DSC)	T_{g1}: 64.03 °C T_{g2}: 64.03 °C ΔH: 67.41 J/g	T_{g1}: 64.75 °C T_{g2}: 107.82 °C ΔH: 51.54 J/g
Gel Time (s)	17 (at 205 °C)	24 (at 205 °C)
Moisture Content (%)	0.21	0.28

Table 4: Control results prior to blasting

Relative Humidity (%)	72,8
Ambient Temperature (^0C)	29,1
Surface Temperature $[T_1]$ (^0C)	72,8
Dew Point $[T_1]$(^0C)	16,8
ΔT Temperature $[T_1 - T_2]$(^0C)	60,2
Pure Water Conductivity ($\mu S/cm$)	3,72
Blasting Media Conductivity ($\mu S/$cm)	8,95
Phosphoric Acid Percentage (%)	6,8

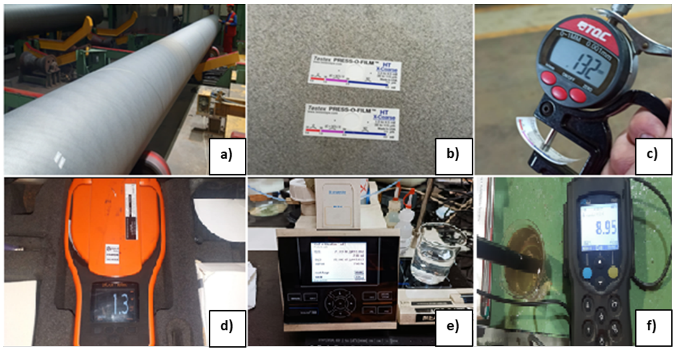

Figure 1: (a) Pipe after sand blasting, (b) roughness tape application on sand blasted pipe, (c) surface roughness measurement, (d) dust test, (e) phosphoric acid ratio determination, (f) blasting media conductivity test

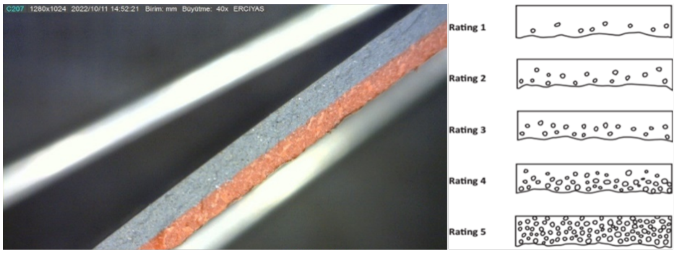

Figure 2: Cross-sectional porosity detection test sample

The blasted surface was examined visually using a comparison catalog in accordance with ISO 8501-1 / SSPC VIS1 standards, and the surface quality was identified as Sa 2.5 / SSPC SP10. The dust level on the blasted surface was measured in accordance with the ISO 8502-3 standard and determined to be the lowest (level 1) [23], [24].

3.2 Physical and Mechanical Test Results

To determine the interface contamination and porosity of the coated pipe, a test sample was cut in the middle and immersed in alcohol at $-30^0 C$for 1 hour. The test sample was removed from the cooling device and compared with the tables in the CSAZ245.20 series 18 standard using a light microscope at 40X magnification. According to the results of this comparison, the interface and section showed level 1 porosity. The interface pollution determination revealed a contamination level of 21 percent. A cross-sectional porosity detection test sample image is shown in Figure 2.

The interface porosity detection test sample image is shown in Figure 3 and the interface contamination detection test sample image is shown in Figure 4. To examine the adhesive strength of the coatings on the metal surface under cold and stress, test samples of 25x200 mm were extracted from the surface of the coated pipe, a bending test was performed under 1.5^0mandrel degree, and crack formation on the coated surfaces was studied. The bending did not cause crack development in the test samples. Table 5 shows the characteristics and results of the bending test samples. Figure 5 depicts an image of the bending test samples.

To determine the impact resistance of the coatings on the metal surface, test samples of 25x200 mm were taken from the surface of the coated pipe and dropped with 1 kg from a height of 15 cm at $-30^0 C$. After dropping 1 kg of weight on the samples, the test temperature was predicted to rise to room temperature. The wet sponge test was carried out with 67.5 volts on test samples whose surface temperature reached room temperature for the control of impact test results. The tested samples were examined and it was found that all of them were suitable, and that following impact with the load, there was no discontinuity

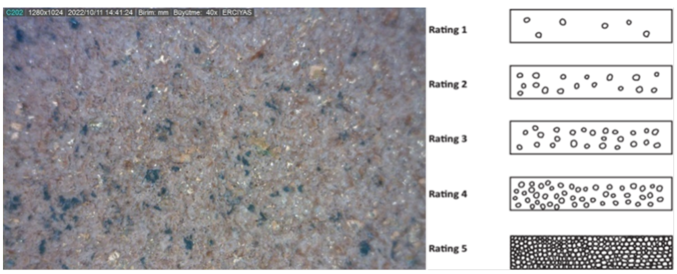

Figure 3: Interfacial porosity detection test sample

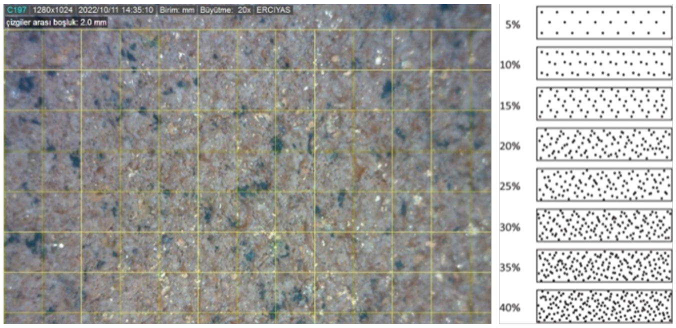

Figure 4: Interfacial contamination detection test sample

Table 5: Bending test sample characteristics and test results

Sample No	Avgerage Dry Film Thickness (µm)	Temperature (°C)	Mandrel Degree (°)	Test Result
1				
2	906,3	-30	1,5	No Crack
3				

that would reach the pipe's surface and generate a spark. The properties and characteristics of the impact test samples are shown in Table 6. The image of the impact test samples is shown in Figure 6.

3.3 Adhesion Test Results

To determine the adhesion strength of metal on the pipe surface using powder epoxy, 100x100 mm samples were cut and removed from the pipe. These samples were stored at 75^0C for 24 hours, as shown in Table 7. An hour later, a 30x15 mm rectangle was opened on the coated surface with a knife, and its corners were checked. Adhesion test findings obtained within the scope of the applicable standard were examined and it was concluded that the results were appropriate. Images of adhesion test samples are shown in Figure 7.

3.4 Cathodic Peeling Test Results

After coating the pipe with powder epoxy resin, 100x100 mm test plates were removed and prepared for cathodic peel testing. The parameters utilized in the cathodic peeling tests are listed in Table 8. When the test results from the adhesion test in Figure 8 are examined, it becomes clear that the values in the relevant specifications and standards are within their tolerances [22], [25].

3.5 Characterization of Coatings

Optical and scanning electron microscopes were used to examine coating and microstructure compatibility, as well as morphological findings. Following the metallographic operations of sanding, polishing, and etching with nital solution,

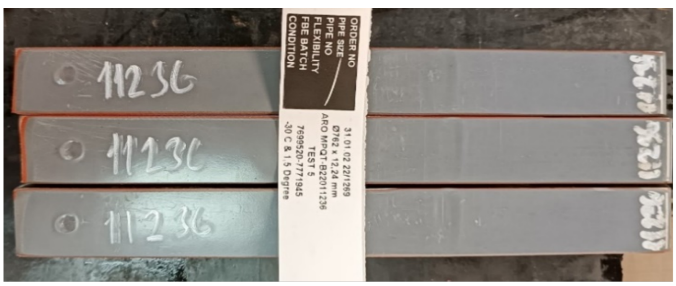

Figure 5: Bending test samples

Table 6: Properties and characteristics of the impact test sample

Sample No	Number of Impact	Temperature (°C)	Test Result
1			
2	5	-30	No discontinuity
3			

Figure 6: Impact test samples

Table 7: Properties and characteristics of the adhesion test sample

Sample No	Temperature (°C)	Time (h)	Adhesion Degree Panel	Acceptance Rating
1				
2	75	24	1 - 1	1 - 3
3				

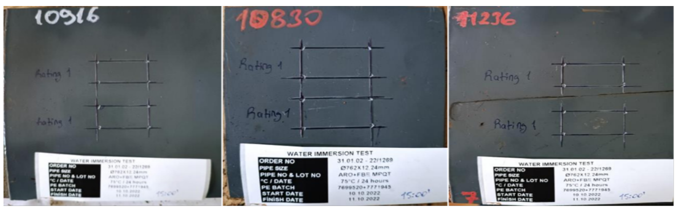

Figure 7: Adhesion test samples

Table 8: Cathodic peeling test parameters and obtained test results

Sample No	1	2	3
Time (h)		24	
Temperature (°C)		65	
Voltage (V)		-3,5	
Maximum Panel Peeling (mm)		0	
Average Panel Peeling (mm		0	
Acceptance Rating (mm)	Max. 11,5		

Figure 8: Cathodic peeling test samples

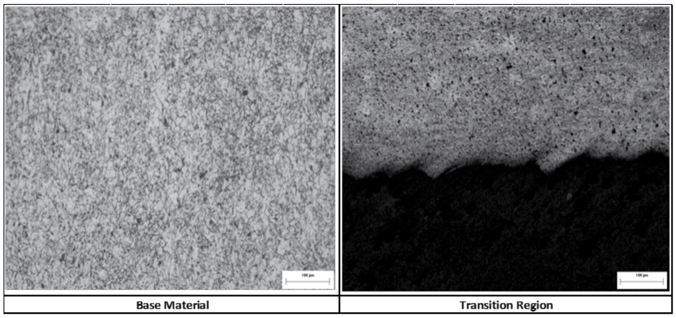

Figure 9: Microstructure of HRC steel after coating at x200 magnification in optical microscope a) base material region, b) steel and coating transition region

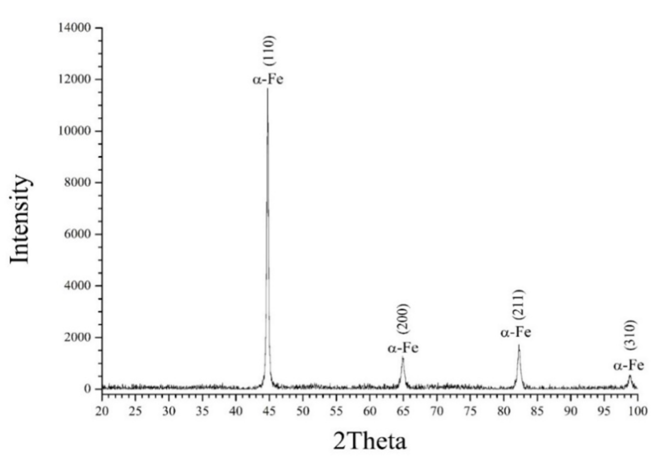

Figure 10: X-Rays diffraction pattern result of HRC steel

respectively, in accordance with the PN-EN ISO 17639:2013-12E standard. The microstructure of HRC steel after the coating process is shown in Figure 9.

The microstructure of HRC steel mainly consists of two phases: polygonal ferrite and granular bainite. It is observed that the microstructure in the transition region has been distorted due to the chemical reaction and heat affect. Thus, polygonal ferrite shape and granular bainite in the main microstructure have disappeared in the transition region. In addition that coated materials have been good compatibility with substrate materials. The effect of void, tear and rupture has been not detected in this region. The coating transitions at the base material-coating interface are smooth [26].

Figure 10 shows the result of the XRD pattern's HRC steel after the coating process due to the high peak intensities of$\alpha - Fe$ phase which has FCC structure, it has dominated in the whole microstructure of HRC Steel. The trace amount of residual austenite could not be detected on the XRD. It was determined by the result of XRD analysis whether there was no phase change or not after the thermal effect and chemical reactions occurring on the surface of the HRC steel during coating. As illustrated in Figure 11, scanning electron microscopy was utilized to distribute these phases [27].

Figure 11 shows the microstructures obtained from the coating and steel interface region from the scanning electron microscope. No adhesion cracks were seen in the coated area. The morphology of the HRC steel more clearly has been seen from the scanning electron microscope. The presence of granular bainite was confirmed at cooling rates below 50°C/s. Granular bainite occurs in steels that are continuously cooled via a mechanism similar to upper bainite (UB). However, due to a more gradual transformation, the beams appear coarse, and carbon enriches the residual austenite during transformation [28]–[31].

4 Conclusions

The feasibility of an FBE+ARO-based coating on steel pipe surfaces was investigated. It was observed that the adhesion and cathodic peeling test, which were used to determine the adhesive and peeling qualities of the coating on the pipe, provided the values in the relevant requirements and standards in tolerances (respectively in accordance with CSA Z245.20-14, TES-CO-FBE-GL standards). In addition, there was no crack and porosity in the coating. The importance of pre-coating and post-coating finishing has been demonstrated in the context of coating characterization. As a result, it has been shown that two-layers of fusion bonded epoxy (FBE+ARO) coating can be used on steel pipe surfaces.

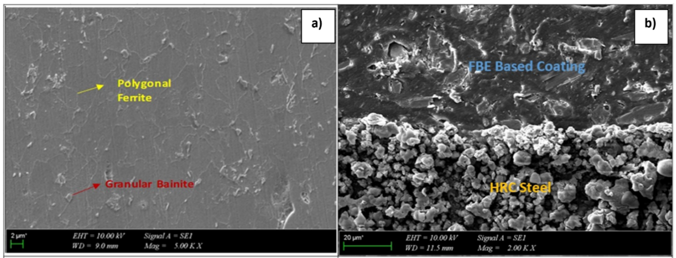

Substrate (a) Interface (b)

Figure 11: SEM analysis results of HRC steel obtained after coating. (a) HRC steel, (b) coating and steel interface

Authors' Contributions

GÇ and MG performed the coating process and performed physical and mechanical tests. SÖ performed the characterization tests. EF wrote up the article in collaboration with other authors. All authors read and approved the final manuscript.

Competing Interests

The authors declare that they have no competing interests.

References

[1] H. Liu, *Pipeline engineering*. CRC Press, 2003.
[2] M. Stewart, "Surface production operations facility piping and pipeline systems: Vol. 3," 2016.
[3] P. Ellenberger, *Piping and pipeline calculations manual: construction, design fabrication and examination*. Elsevier, 2014.
[4] A. Dinita and S. Kolisnychenko, *Corrosion. Tube Products and Pipeline Systems*. Trans Tech Publications Ltd, 2021.
[5] D. Kuang and F. Cheng, "Coating degradation in the presence of alternating current interference," in *NACE CORROSION*. NACE, 2016.
[6] W. K. Muhlbauer, *Pipeline risk management manual: ideas, techniques, and resources*. Elsevier, 2004.
[7] E. S. Menon, *Pipeline planning and construction field manual*. Gulf Professional Publishing, 1978.
[8] Y. Bai and Q. Bai, *Subsea pipeline integrity and risk management*. Gulf Professional Publishing, 2014.
[9] R. Singh, *Pipeline Integrity: Management and Risk Evaluation*. Gulf Professional Publishing, 2017.
[10] M. S. Okyere, *Mitigation of Gas Pipeline Integrity Problems*. CRC Press, 2020.
[11] P. Hopkins, "The skills crisis in the pipeline sector of the oil and gas business," *Journal of Pipeline Engineering*, vol. 7, no. 3, pp. 1–55, 2008.
[12] D. Alkazraji, *A quick guide to pipeline Engineering*. Elsevier, 2008.
[13] A. C. Palmer and R. A. King, *Subsea pipeline engineering*. PennWell Books, 2008.
[14] E. McAllister, *Pipe Line Rules of Thumb Handbook*. Elsevier, 1993.
[15] J. N. Tiratsoo and J. Tiratsoo, *Pipeline pigging technology*. Gulf Professional Publishing, 1992.
[16] R. R. Fessler, "Pipeline corrosion," *Report, US Department of Transportation Pipeline and Hazardous Materials Safety Administration, Baker, Evanston, IL*, 2008.
[17] K. Escoe, *Piping and pipelines assessment guide*. Elsevier, 2006, vol. 1.
[18] M. Orazem, *Underground pipeline corrosion*. Elsevier, 2014, no. 63.
[19] M. Mohitpour, A. Murray, M. McManus, and I. Colquhoun, *Pipeline integrity assurance: a practical approach*. ASME Press, 2010.
[20] E. Altuncu, Ç. Gökhan, and G. Mahmut, "Spiral kaynaklı çelik boruların korozyona karşı fbe kaplamaların test ve karakterizasyonu," *El-Cezeri*, vol. 7, no. 2, pp. 679–689, 2020.
[21] J. Been and J. Wolodko, "Comparison of the corrosivity of dilbit and conventional crude," *Report of Alberta Innovates Technology Futures*, 2011.
[22] "Plant-applied external fusion bond epoxy coating for steel pipe (LEFM) approach," Canadian Standards Association, Canada, Standard, 2018.
[23] "Çelik taban malzeme yüzeylerin hazırlanması (G_{IC} and K_{IC}) Bolum 1," TSE, Standard, 2008.
[24] "Çelik yüzeylerin hazırlanması (G_{IC} and K_{IC}) Bolum 3," TSE, Standard, 2017.
[25] "External fusion bond epoxy for steel pipe specification (LEFM) approach," Trans Canada Engineering, Specification, 2017.
[26] A. Roccisano, S. Nafisi, D. Stalheim, and R. Ghomashchi, "Effect of tmcp rolling schedules on the microstructure and performance of x70 steel," *Materials Characterization*, vol. 178, p. 111207, 2021.
[27] A. Mostafapour, A. Ebrahimpour, and T. Saied, "Identification of retained austenite, ferrite, bainite and martensite in the microstructure of trip steel," *International journal of iron and steel society of Iran*, vol. 13, no. 2, pp. 1–6, 2016.
[28] K. Kobayashi and K. Takewaka, "Experimental studies on epoxy coated reinforcing steel for corrosion protection," *International Journal of Cement Composites and Lightweight Concrete*, vol. 6, no. 2, pp. 99–116, 1984.
[29] Z.-X. Gui, K. Wang, Y.-S. Zhang, and B. Zhu, "Cracking and interfacial debonding of the al–si coating in hot stamping of pre-coated boron steel," *Applied surface science*, vol. 316, pp. 595–603, 2014.
[30] S. Zajac, V. Schwinn, and K. Tacke, "Characterisation and quantification of complex bainitic microstructures in high and ultra-high strength linepipe steels," in *Materials Science Forum*, vol. 500. Trans Tech Publ, 2005, pp. 387–394.
[31] G. Song, W. G. Sloof, T. Vystavel, and J. T. de Hosson, "Interface microstructure and adhesion of zinc coatings on trip steels," in *Materials science forum*, vol. 539. Trans Tech Publ, 2007, pp. 1104–1109.